

## MR-elastography reveals degradation of tissue integrity in multiple sclerosis

Jens Wuerfel<sup>a,e,\*</sup>, Friedemann Paul<sup>a</sup>, Bernd Beierbach<sup>b</sup>, Uwe Hamhaber<sup>c</sup>, Dieter Klatt<sup>b</sup>, Sebastian Papazoglou<sup>b</sup>, Frauke Zipp<sup>a</sup>, Peter Martus<sup>d</sup>, Jürgen Braun<sup>c</sup>, Ingolf Sack<sup>b,\*</sup>

<sup>a</sup> Cecilie Vogt Clinic for Neurology, Charité - University Medicine Berlin and Max-Delbrueck Center for Molecular Medicine, Berlin, Germany

<sup>b</sup> Department of Radiology, Charité - University Medicine Berlin, Campus Charité Mitte, Berlin, Germany

<sup>c</sup> Institute of Medical Informatics, Charité - University Medicine Berlin, Campus Benjamin Franklin, Berlin, Germany

<sup>d</sup> Institute of Biometry and Clinical Epidemiology, Charité - University Medicine Berlin, Campus Benjamin Franklin, Berlin, Germany

<sup>e</sup> Institute of Neuroradiology; University Luebeck; Germany

### ARTICLE INFO

#### Article history:

Received 8 March 2009

Revised 5 June 2009

Accepted 8 June 2009

Available online 16 June 2009

#### Keywords:

Multiple sclerosis

MRI

Magnetic resonance elastography

Viscoelasticity

Brain

Gender

### ABSTRACT

In multiple sclerosis (MS), diffuse brain parenchymal damage exceeding focal inflammation is increasingly recognized to be present from the very onset of the disease, and, although occult to conventional imaging techniques, may present a major cause of permanent neurological disability. Subtle tissue alterations significantly influence biomechanical properties given by stiffness and internal friction, that – in more accessible organs than the brain – are traditionally assessed by manual palpation during the clinical exam. The brain, however, is protected from our sense of touch, and thus our current knowledge on cerebral viscoelasticity is very limited. We developed a clinically feasible magnetic resonance elastography setup sensitive to subtle alterations of brain parenchymal biomechanical properties. Investigating 45 MS patients revealed a significant decrease (13%,  $P < 0.001$ ) of cerebral viscoelasticity compared to matched healthy volunteers, indicating a widespread tissue integrity degradation, while structure-geometry defining parameters remained unchanged. Cerebral viscoelasticity may represent a novel *in vivo* marker of neuroinflammatory and neurodegenerative pathology.

© 2009 Elsevier Inc. All rights reserved.

### Introduction

The pathologic hallmarks of multiple sclerosis (MS) are inflammatory foci with demyelination, axonal degeneration, and reactive gliosis (Pitcock and Lucchinetti, 2007). Although magnetic resonance imaging (MRI) has become the most important paraclinical tool for diagnosis and monitoring of MS, conventional MRI parameters correlate only modestly with the clinical course and neurological disability (Barkhof, 2002). Thus, new imaging modalities that provide a more specific measure of *in vivo* histopathological and cellular aspects of the disease process are needed (Miller et al., 2003). A direct measure of the tissue constitution could be based on the assessment of cell adhesion and tissue scaffold rigidity by measuring the macroscopic viscoelasticity of the brain parenchyma (Fung, 1993). Tactile measures of viscoelasticity are, for example, the stiffness or the softness of a given tissue, that can be obtained by simple palpation, as

routinely employed during the physical examinations. The brain, however, is protected from our sense of touch, limiting the present knowledge on *in vivo* cerebral viscoelasticity and its relation to central nervous system pathologies. In a technical “palpation”, known as magnetic resonance elastography (MRE), shear waves are applied with frequencies at the acoustic range, and a phase-sensitive MR sequence is used to detect propagating waves (Muthupillai and Ehman, 1996). Elastographic techniques have previously shown a high sensitivity for detecting subtle tissue alterations in skeletal muscle (Basford et al., 2002; Papazoglou et al., 2006), breast (McKnight et al., 2002; Sinkus et al., 2007) and liver (Asbach et al., 2008) pathologies. Cerebral MRE provides a unique tool measuring the viscoelasticity of brain parenchyma in its intact physiological environment (Kruse et al., 2008; Sack et al., 2008), circumventing the natural mechanical shielding through the skull, cerebrospinal fluid, and meninges. We recently developed a novel sensitive and highly reproducible setup that allows the calculation of global cerebral shear moduli and shear viscosities, based on a head-rocker actuator, the fast acquisition of scalar wave fields using echo planar imaging (EPI), and the analysis of complex-modulus inversion of time-resolved wave images (Sack et al., 2008). Here we investigated the potential of cerebral MRE to detect subtle diffuse parenchymal damage in mildly affected MS patients, that is not represented by macroscopically visible lesions.

\* Corresponding authors. I. Sack is to be contacted at Department of Radiology, Charité - Universitätsmedizin Berlin, Charitéplatz 1, 10117 Berlin, Germany. J. Wuerfel, Institute of Neuroradiology, University Luebeck, Ratzeburger Allee 160, 23568 Luebeck, Germany.

E-mail addresses: [jens.wuerfel@uk-sh.de](mailto:jens.wuerfel@uk-sh.de) (J. Wuerfel), [ingolf.sack@charite.de](mailto:ingolf.sack@charite.de) (I. Sack).

**Patients and methods**

We determined the complex modulus ( $G$ ) in 79 participants, comprising 45 MS patients with mild relapsing-remitting disease course (mean Expanded Disability Status Score (EDSS) 1.6; range 0–4), and 34 age and gender matched healthy volunteers without neurological or psychiatric conditions, as presented in Table 1. The study was approved by the local ethics committee, and written informed consent was obtained from all subjects. Principles of our assay are presented in Fig. 1.

Every participant underwent an MRE examination of approximately 15 min duration in a standard 1.5 T-clinical MRI scanner (Siemens, Erlangen, Germany) in addition to a routine clinical MRI protocol: T2-weighted images (repetition time (TR): 5780 ms, echo-time (TE): 81 ms, 3 mm slice thickness and 44 contiguous axial slices).

In patients, conventional spin-echo T1-weighted images (TR: 1060 ms, TE: 14 ms, 3 mm slice thickness and 44 contiguous axial slices) were obtained before and 5 min after injection of 0.1 mmol/kg Gd-DTPA (gadopentate dimeglumine (Magnevist®), Bayer-Schering, Berlin, Germany). Blinded MRI data analysis was performed of conventional MRI data, following a semi-automatic procedure, which included an image coregistration (Jenkinson et al., 2002) as well as an inhomogeneity correction routine embedded into the MedX3.4.3 software package (Medical Numerics, Germantown, USA). Bulk white matter lesion load of T2-weighted scans as well as number and volume of hyperintense lesions on T1-weighted scans were routinely measured using the MedX v.3.4.3 software package, as described previously (Wuerfel et al., 2004, 2008). Brain parenchymal fraction (BPF) was calculated applying a fully automated software tool (Smith et al., 2002). In 16 healthy volunteers (5 females), a three-dimensional T1-weighted sequence (MPRAGE, TR: 2110 ms, TE:

4.38 ms, flip angle 15°, isotropic resolution 1 mm<sup>3</sup>) replaced conventional spin-echo T1-weighted images.

The MRE protocol comprised a single-shot spin-echo echo planar imaging sequence with a sinusoidal motion-encoding gradient (MEG) in through-plane direction that was used to acquire three transversal image slices in a central slab through the cerebrum (Number of MEG cycles: 4, MEG amplitude: 35 mT/m, TR: 3.0 s, echo-time TE: 149 ms, field of view (FoV): 192 × 192 mm<sup>2</sup>, matrix size: 128 × 128, slice thickness: 6 mm). The acquisition was repeated eighty times for each image slice with an alternating sign of motion sensitization, and an increasing delay between the onset of vibration and the motion-encoding.

A multifrequency vibration with a maximum amplitude of approximately 1 mm in parallel direction to the long axis of the magnet was fed into an actuator by a carbon-fiber piston. The resulting time-resolved wave images,  $u(x,y,t)$  (with  $x$  and  $y$  as spatial coordinates), were Fourier-transformed for decomposition into complex wave images at driving frequency:  $U(x,y,\omega)$ , ( $\omega/2\pi = 25, 37.5, 50$  and  $62.5$  Hz). Complex modulus images were obtained by wave inversion ( $G(x,y,\omega) = -\rho\omega^2 U/\Delta U$ , with  $\Delta$  as the Laplace operator and  $\rho$  being the tissue's density of 1 kg/dm<sup>3</sup>), spatially averaged within the segmented brain parenchyma and displayed on image slices (Fig. 2A). The resulting global modulus function was fitted by a least-square routine. A good match between model and multifrequency data was achieved by a combination of Voigt and Maxwell models given by the Zener model. However, the latter model incorporated an additional parameter – a second shear modulus – rendering the interpretation of viscoelastic constants rather cumbersome. The optimal tradeoff between physical significance and representation of the frequency dependency of our data was achieved by a two-parameter springpot model  $G = \kappa(\omega f)^\alpha$  that interpolated between springs and dashpots introducing a fractional element  $\kappa = \mu^{1-\alpha} f^\alpha$ , as also shown previously on healthy volunteers (Sack et al., 2009b). The

**Table 1**  
Classification of 79 subjects included in our study with resulting viscoelastic parameters according to the springpot model.

	All subjects		Females		Males	
	MS	Controls	MS	Controls	MS	Controls
Number of individuals	45	34	23	17	22	17
Age						
Mean	37.84	37.00	37.8	34.5	37.9	39.5
Median	38	37	39	37	38	38
Range (in years)	21–51	18–59	22–50	18–55	21–51	21–59
CEL count						
Mean	0.6	–	0.9	–	0.3	–
SD	1.5	–	1.7	–	1.3	–
Range	0–6	–	0–6	–	0–6	–
CEL vol. (ml)						
Mean	33.8	–	55.1	–	11.5	–
SD	86.2	–	107.4	–	49.7	–
Range	0–351	–	0–351	–	0–228	–
T2 lesion vol. (ml)						
Mean	3870	–	3511	–	3906	–
SD	3312	–	3237	–	3457	–
Range	25–11036	–	25–11036	–	61–9194	–
T2 les. count						
Mean	17.7	–	18.9	–	16.5	–
SD	11.8	–	15.0	–	11.5	–
Range	4–46	–	5–38	–	4–46	–
BPF						
Mean	0.8579	–	0.8543	–	0.8628	–
SD	0.0241	–	0.0218	–	0.0269	–
Range	0.7885–0.8939	–	0.8069–0.8939	–	0.7885–0.8939	–
Mean structural Parameter $\alpha$	0.266 (0.009)	0.266 (0.010)	0.267 (0.009)	0.267 (0.009)	0.266 (0.009)	0.265 (0.011)
Mean viscoelasticity $\mu$ (in Pa)	1865 (251)	2137 (314)	1875 (256)	2266 (307)	1853 (252)	2008 (271)
$\Delta\mu$	273 Pa		391 Pa		155 Pa	
	13%		17%		8%	
	$P < 0.001$		$P < 0.001$		$P = 0.07$	

Tolerances given in brackets refer to the standard deviation.  $\Delta\mu$  denotes age-adjusted differences in elasticity given by  $\mu$  (MS) minus  $\mu$  (controls). CEL = contrast enhancing T1-hyperintense lesions. BPF = brain parenchymal fraction.

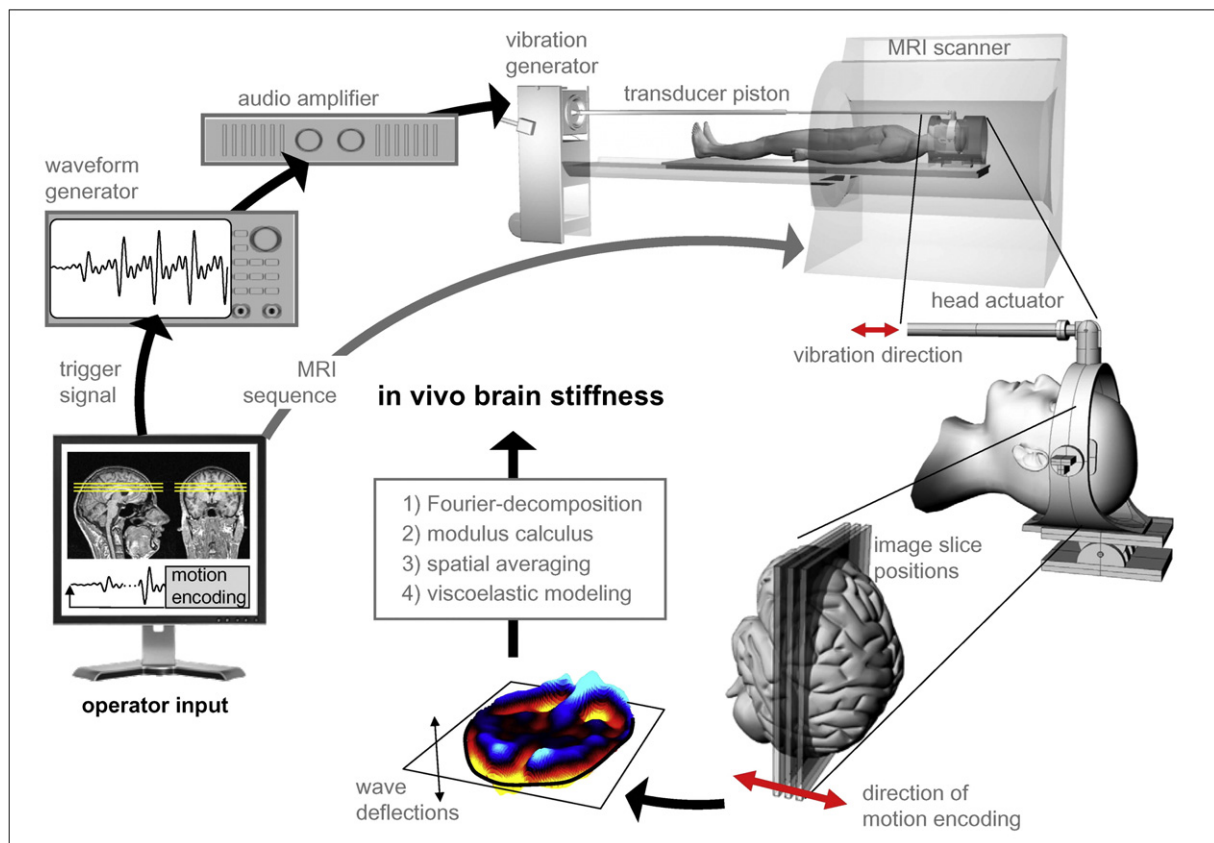


**Fig. 1.** Apparatus and key technical points of the *in vivo* assay for brain-stiffness measurements. The host computer (lower left corner) controls the MRI scanner and the wave generator. The operator selects image slice position, direction, amplitude and timing of motion-encoding. The onset of the multifrequency vibration is triggered by the MRI sequence approximately 400 ms prior to motion-encoding. A variation of this delay allows a temporal resolution of the propagation of the shear waves through the brain. As a mechanical stimulus, a superposition of four frequencies from 25 to 62.5 Hz is generated by a loudspeaker and transferred by a rigid piston to a head cradle. The resulting intracranial shear waves are captured and processed according to steps 1) through 4).

viscoelastic variable  $\kappa$  and the structural parameter  $\alpha$  were deduced from eight independent measures ( $G'$  and  $G''$  at four vibration frequencies, see Fig. 2B). Henceforth, the springpot was considered our reference two-parameter model. As  $\kappa$  has a rather complicated dimension of  $\text{Pa}^{(1-\alpha)}$  ( $\text{Pa s}$ ) $^\alpha$ , we transformed this mixed viscoelastic constant to the parameter related to shear elasticity  $\mu$ . In contrast to the mean viscosity, which we previously determined with a higher-order viscoelastic model (Zener model) on a smaller sample (Asbach et al., 2008; Klatt et al., 2007), the applied value  $\eta = 3.7 \text{ Pa s}$  corresponded to a large cohort of healthy volunteers covering a broad age range (Sack et al., 2009b). Of note, the transformation of  $\kappa$  to the elasticity modulus  $\mu$  did not impact the statistical significance of our data, but rendered the derived viscoelastic quantities comparable to previous studies of brain MRE (Sack et al., 2008).

All MRI experiments were carried out at the same time of the day, in order to rule out possible side effects by the hydration state of the investigated subjects.

#### Statistical data analysis

Four storage moduli  $G'$ , four loss moduli  $G''$  and two constitutive parameters  $\alpha$  and  $\mu$  were analyzed for each participant. Moduli  $G'$  and  $G''$  as well as the viscoelasticity  $\mu$  were highly correlated and showed comparable results. All data were distributed approximately normally. For all correlation analyses a two-sided Spearman rank correlation coefficient was applied. The level of significance was 0.05; all analyses were carried out using SPSS for Windows (release 15.0).

## Results

### Brain parenchymal viscoelasticity is significantly reduced in MS patients

We observed significantly reduced global brain parenchymal viscoelasticity ( $\mu$ ) in MS patients compared to matched controls (13%,  $P < 0.001$ ; Table 1). Biomechanical properties of the brain parenchyma could be safely and routinely quantified *in vivo* applying our novel device that imposed almost no burden on volunteers and patients (Fig. 1): none of 79 investigated individuals felt uncomfortable during the measurements. Brain parenchymal viscoelasticity was not correlated to conventional MRI measures of the “disease burden” such as T2-hyperintense lesion load, blood brain barrier breakdown, or brain parenchymal fraction (Table 1). In our cohort, the clinical disability represented by the EDSS was only dependent from the duration of disease; none of the imaging parameters showed significant correlations with the EDSS. Of note, the disease related reductions of brain parenchymal viscoelasticity were most prominent in female patients (17%,  $P < 0.001$ ; Fig. 3). Conventional MRI measures of the “disease burden” could not differentiate women from men (Table 1), nor was brain volume a co-factor of viscoelasticity ( $P = 0.25$ ). This was also indicated by high  $\mu$  in women, which is reciprocal to the gender disparity of brain volumes in general (Franklin et al., 2000). The conclusion was supported by the fact that the observed disease dependency of the complex modulus  $G$  did not change with drive frequency (Table 2).

When further accounting for gender aspects, we also detected marked differences in healthy volunteers: female brains were 11% stiffer than

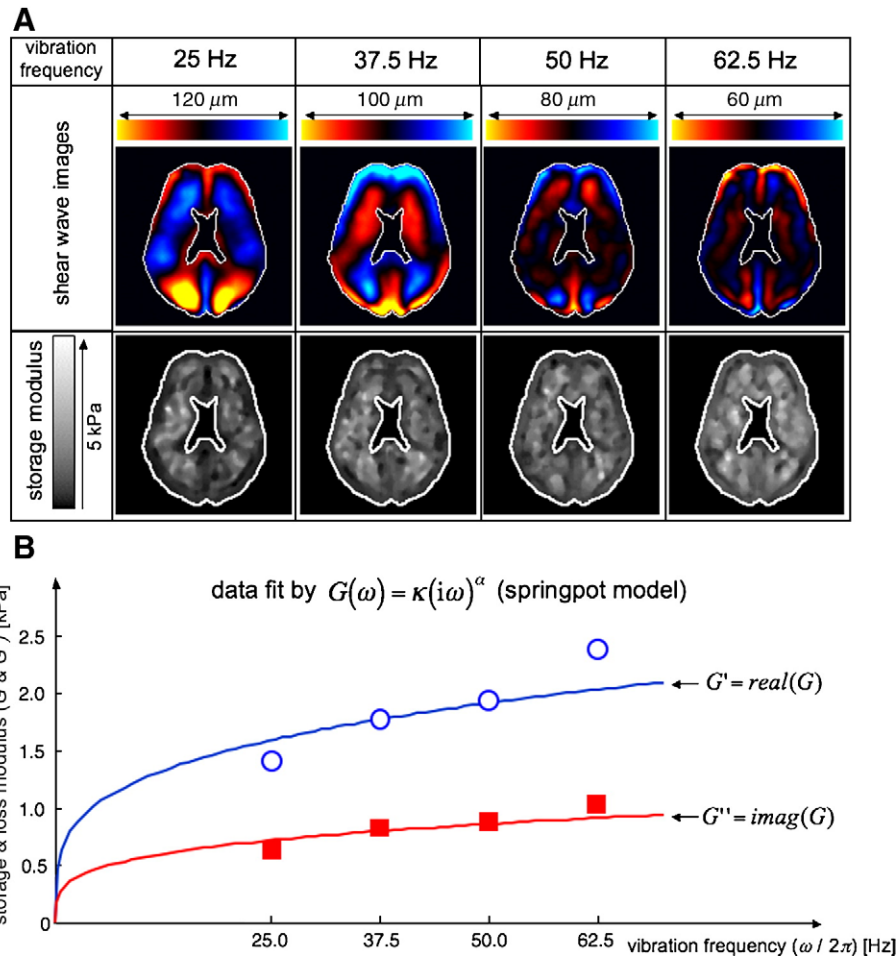


**Fig. 2.** A: Example of MRE image data. Four principle harmonics were received after Fourier decomposition corresponding to the waveform fed into the driver. Wave inversion was used to calculate the complex modulus  $G(\omega)$  from wave images characterizing the material's viscoelasticity. The storage modulus is shown as calculated from the wave images above. B: Spatial variations in G-images were averaged yielding four complex moduli per individual, represented as  $G'$  and  $G''$  on a frequency axis. Blue data points (circles) and the fitted curve correspond to  $G'$ , while red squares and the red fitted curve represent  $G''$ . The fit function is a two-parameter power law with a structural parameter  $\alpha$  and a viscoelastic constant  $\kappa$ . The latter is ascribed to the viscoelasticity assuming a specific viscosity of brain tissue.

those of their age-matched male counterparts ( $P < 0.01$ ). Remarkably, we did neither find an interaction of  $\alpha$  with MS nor with gender. This is in good agreement with our observation of a corresponding decline

of storage and loss moduli  $G'$  and  $G''$  (Table 2) indicating an MS-related decline of both, elasticity and viscosity.

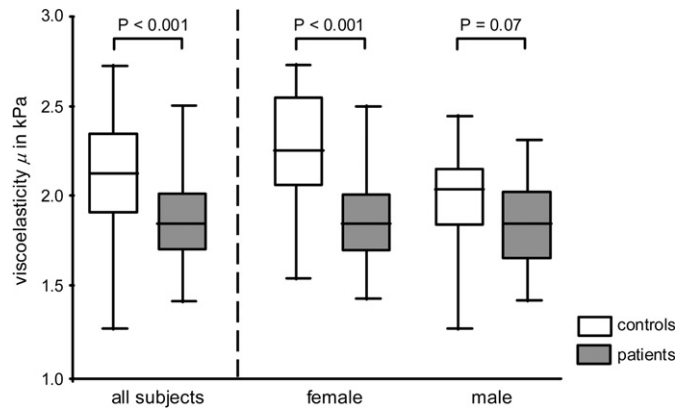


**Fig. 3.** Women presented with stiffer brains but also higher susceptibility to MS induced viscoelasticity changes compared to men. Gender differences of cerebral mean viscoelasticity  $\mu$  (kPa) in MS patients and matched healthy individuals, corresponding to the springpot model calculation. The boxplot depicts the lower and upper quartiles as well as the 50th percentile (median). Full data range is presented by the whiskers.

### Discussion

Neuronal and axonal degeneration, as well as damage to myelin sheaths, incomplete remyelination and reduction of mature oligodendrocytes, all of which are typical histopathological findings in MS (Pittock and Lucchinetti, 2007; Zipp and Aktas, 2006), may contribute to the loss of tissue integrity in neuroinflammatory and neurodegenerative diseases.

Our findings of reduced viscoelasticity in MS patients raise the question on how neurons or glial cells contribute to the general mechanical properties of the brain. Reactive astrogliosis is a key feature of neuroinflammatory diseases. Glial cells were recently characterized to be biomechanically less rigid compared to neurons (Lu et al., 2006), which is consistent with our *in vivo* results, but contradicts a previous notion of glia representing a predominant mechanical scaffold for neurons. Clearly, our tentative interpretation of the detected brain-stiffness alterations does not account for elaborate cellular force-feedback loops given by the active and nonlinear response of cells to a changing mechanical environment (Discher et al., 2005; Van Essen, 1997). Such nonlinear responses have been described for cytoskeletal rigidity, adhesion, and other cellular

**Table 2**  
Unmodelled brain viscoelasticity at four drive frequencies of 25, 37.5, 50 and 62.5 Hz.

Modulus	All subjects		Females		Males	
	MS	Controls	MS	Controls	MS	Controls
$G'$ (25 Hz)	1052 (146)	1216 (159)	1050 (147)	1265 (149)	1054 (307)	1167 (156)
$\Delta$	–164 Pa 13% $P < 0.001$		–215 Pa 17% $P < 0.001$		–113 Pa –9% $P < 0.05$	
$G'$ (37.5 Hz)	1275 (203)	1423 (265)	1261 (182)	1518 (254)	1289 (227)	1328 (248)
$\Delta$	–148 Pa –10% $P < 0.01$		–257 Pa –17% $P < 0.01$		–40 Pa –3% $P = 0.25$	
$G'$ (50 Hz)	1472 (148)	1631 (187)	1488 (151)	1706 (174)	1455 (147)	1555 (172)
$\Delta$	–159 Pa –10% $P < 0.001$		–218 Pa –13% $P < 0.001$		–100 Pa –6% $P = 0.06$	
$G'$ (62.5 Hz)	1974 (154)	2109 (171)	1982 (163)	2176 (166)	1965 (148)	2042 (152)
$\Delta$	–135 Pa –6% $P < 0.001$		–195 Pa –9% $P < 0.001$		–76 Pa –4% $P = 0.12$	
$G''$ (25 Hz)	462 (65)	538 (77)	460 (60)	561 (77)	464 (71)	515 (72)
$\Delta$	–76 Pa –14% $P < 0.001$		–101 Pa –18% $P < 0.001$		–51 Pa –10% $P < 0.05$	
$G''$ (37.5 Hz)	576 (100)	638 (114)	566 (88)	679 (104)	587 (112)	598 (112)
$\Delta$	–62 Pa –10% $P < 0.05$		–113 Pa –17% $P < 0.01$		–11 Pa –2% $P = 0.77$	
$G''$ (50 Hz)	579 (70)	649 (92)	582 (68)	676 (86)	575 (73)	622 (93)
$\Delta$	–70 Pa –11% $P < 0.001$		–94 Pa –14% $P < 0.001$		–47 Pa –7% $P = 0.09$	
$G''$ (62.5 Hz)	777 (78)	854 (104)	789 (84)	896 (98)	765 (71)	812 (94)
$\Delta$	–77 Pa –9% $P < 0.001$		–107 Pa –12% $P < 0.001$		–47 Pa –6% $P = 0.09$	

The storage and loss moduli ( $G'$  and  $G''$ ) and their interindividual standard deviations (in brackets) are given in units of Pa.  $\Delta$  refers to the difference between cohorts (MS – healthy volunteers).

processes which may cause a viscoelastic “hyper-response” of the brain, exceeding the effects of CNS pathology identified by conventional MRI (Barkhof, 2002; Mueller et al., 2006).

The main challenge of cerebral MRE is the mechanical brain stimulation, which is naturally restricted by the almost perfect shielding of the brain against shear deformations, hindering sufficient intracranial wave amplitudes. We here present a clinically applicable, safe and comfortable device that imposed almost no burden on volunteers and patients. In our model, the order of magnitude of viscoelastic parameters determines the solid–fluid behavior, the liquefaction or the cohesiveness of tissue – namely the *tissue integrity* – and is measured by the elasticity modulus  $\mu$ . On the other hand, the interpolation factor  $\alpha$  between a purely elastic material (modelled by a spring;  $\alpha = 0$ ) and a purely viscous material (modelled by a dashpot;  $\alpha = 1$ ) characterizes the *geometry of the tissue structure* or the geometrical cytoarchitecture. In a figurative translation, this parameter represents the relative number of springs and dashpots as well as their hypothetical alignment. In that sense  $\alpha$  is a structural parameter related to the geometry and the composition of tissue building components. In contrast,  $\kappa$  quantifies the spring constants and the coefficients of energy loss at a given arrangement of element models indicating the solidity or fluidity of the measured tissue. Since both, elasticity and viscosity, are linearly dependent in  $\kappa$ , we could replace  $\kappa$  by the elasticity modulus  $\mu$  assuming a specific viscosity, which transfers the arbitrary solid–fluid scale given by  $\kappa$  to the order of elasticity observed in living human brain.

In our experiments,  $\mu$  did not correlate with brain volume changes which is in accordance to findings of a recent study performed on healthy volunteers (Sack et al., 2009b). In contrast, wave reflections and diffractions at sites of tissue boundaries are highly frequency dependent (Papazoglou et al., 2007; Papazoglou et al., 2008). Thus, a decrease in the brain parenchymal fraction (BPF), which is expressed

by an increase in ventricle volume and sulci size, would result in different BPF effects at different driving frequencies. The fact that this was not observed in our data provides strong evidence that MRE is stable against effects related to tissue boundaries and interfaces. It is important to note that this conclusion can only be drawn for the proposed *global* approach in brain MRE. Averaging the brain parenchymal modulus-values of three image slices reduced the inherent susceptibility of wave inversion algorithms to noise and boundary problems (Papazoglou et al., 2008). On the other hand, this technical constraint prevented us from analyzing local moduli as well as possible viscoelasticity differences between normal appearing white matter and MS lesions.

Scalar wave fields were acquired based upon MRE-studies of phantoms (Papazoglou et al., 2008), liver (Yin et al., 2007; Klatt et al., 2006) and brain (Sack et al., 2008, 2009a) which demonstrated the reproducibility of the deduced isotropic moduli measured in a very time-efficient way. The ‘isotropic’ moduli of brain parenchyma presented here compensate for spatial heterogeneity and anisotropic elastic coefficients. Heterogeneity results in multiple fibre orientations within the white matter. Shear rheometer tests of  $10 \times 5 \times 1 \text{ mm}^3$  brain samples revealed a significantly higher shear modulus along the fibers ( $\times 1.93$ ) than perpendicular only inside the corpus callosum (Prange and Margulies, 2002). The current spatial resolution in MRE (after wave inversion) still exceeds these dimensions and would therefore not allow for a reliable analysis of the mechanical anisotropy of the brain.

It appears worthwhile to contrast fibrous liver disease as biomechanical counter-system to MS: the viscoelasticity of the liver increases by connective tissue proliferation during fibrosis, while the ratio of elasticity and viscosity remains widely unchanged (Asbach et al., 2008), giving rise to a constant structural parameter  $\alpha$ . Thus, pathological hepatic stiffening as well as liquefaction of the brain

detected by MRE are less dependent on the remodeling of the organ's geometrical cytoarchitecture but rather are associated with integrity or degradation of structure-determining tissue. In our cohort, MRI parameters including viscoelasticity were not correlated with the disability score expressed by the EDSS. However, future studies investigating more sophisticated clinical disease measures such as the multiple sclerosis functional composite (MSFC) as well as longitudinal data may contribute to solve the clinico-radiological paradox in MS. Although a “gender gap” of women being two to three times more likely to develop MS compared to men is well perceived (McCarthy, 2000), little is known about cytoarchitectural brain gender differences, and thus their impact on MS pathophysiology remains speculative. Irrespective of histopathological evidence supporting our results, we propose that viscoelastic properties could be developed as future surrogate markers, equivalent to clinical findings derived from palpation of other more accessible organs. Other emerging imaging technologies including higher magnetic field strengths, proton spectroscopy, diffusion tensor imaging or magnetization transfer imaging may complement our findings of *in vivo* biomechanical tissue alterations.

Cerebral MRE provides a novel and sensitive technique for the early detection of subtle alterations in viscoelastic cerebral tissue properties. It may contribute as a valuable and clinically applicable *in vivo* imaging tool to diagnosis, monitoring and evaluation of therapeutic strategies in neuroinflammatory and neurodegenerative diseases.

### Acknowledgments

We thank Martina Paetzel for carefully editing this manuscript as native English speaker. The authors have no conflict of interests to declare.

Grant support: German Research Foundation (Sa / 901-3).

### References

- Asbach, P., Klatt, D., Hamhaber, U., Braun, J., Somasundaram, R., Hamm, B., et al., 2008. Assessment of liver viscoelasticity using multifrequency MR elastography. *Magn. Reson. Med.* 60, 373–379.
- Barkhof, F., 2002. The clinico-radiological paradox in multiple sclerosis revisited. *Curr. Opin. Neurol.* 15, 239–245.
- Basford, J.R., Jenkyn, T.R., An, K.N., Ehman, R.L., Heers, G., Kaufman, K.R., 2002. Evaluation of healthy and diseased muscle with magnetic resonance elastography. *Arch. Phys. Med. Rehabil.* 83, 1530–1536.
- Discher, D.E., Janmey, P., Wang, Y.L., 2005. Tissue cells feel and respond to the stiffness of their substrate. *Science* 310, 1139–1143.
- Franklin, M.S., Kraemer, G.W., Shelton, S.E., Baker, E., Kalin, N.H., Uno, H., 2000. Gender differences in brain volume and size of corpus callosum and amygdala of rhesus monkey measured from MRI images. *Brain Res.* 852, 263–267.
- Fung, Y., 1993. *Biomechanics: Mechanical Properties of Living Tissue*. Springer-Verlag, New York.
- Jenkinson, M., Bannister, P., Brady, M., Smith, S., 2002. Improved optimization for the robust and accurate linear registration and motion correction of brain images. *NeuroImage* 17, 825–841.
- Klatt, D., Asbach, P., Rump, J., Papazoglou, S., Somasundaram, R., Modrow, J., et al., 2006. *In vivo* determination of hepatic stiffness using steady-state free precession magnetic resonance elastography. *Invest. Radiol.* 41, 841–848.
- Klatt, D., Hamhaber, U., Asbach, P., Braun, J., Sack, I., 2007. Noninvasive assessment of the rheological behavior of human internal organs using multifrequency MR elastography: a study of brain and liver viscoelasticity. *Phys. Med. Biol.* 52, 7281–7294.
- Kruse, S.A., Rose, G.H., Glaser, K.J., Manduca, A., Felmlee, J.P., Jack Jr., C.R., et al., 2008. Magnetic resonance elastography of the brain. *NeuroImage* 39, 231–237.
- Lu, Y.B., Franze, K., Seifert, G., Steinhauser, C., Kirchhoff, F., Wolburg, H., et al., 2006. Viscoelastic properties of individual glial cells and neurons in the CNS. *Proc. Natl. Acad. Sci. U. S. A.* 103, 17759–17764.
- McCarthy, M., 2000. The “gender gap” in autoimmune disease. *Lancet* 356, 1088.
- McKnight, A.L., Kugel, J.L., Rossman, P.J., Manduca, A., Hartmann, L.C., Ehman, R.L., 2002. MR elastography of breast cancer: preliminary results. *AJR Am. J. Roentgenol.* 178, 1411–1417.
- Miller, D.H., Thompson, A.J., Filippi, M., 2003. Magnetic resonance studies of abnormalities in the normal appearing white matter and grey matter in multiple sclerosis. *J. Neurol.* 250, 1407–1419.
- Mueller, S.G., Schuff, N., Weiner, M.W., 2006. Evaluation of treatment effects in Alzheimer's and other neurodegenerative diseases by MRI and MRS. *NMR Biomed.* 19, 655–668.
- Muthupillai, R., Ehman, R.L., 1996. Magnetic resonance elastography. *Nat. Med.* 2, 601–603.
- Papazoglou, S., Rump, J., Braun, J., Sack, I., 2006. Shear-wave group-velocity inversion in MR elastography of human skeletal muscle. *Magn. Reson. Med.* 56, 489–497.
- Papazoglou, S., Hamhaber, U., Braun, J., Sack, I., 2007. Horizontal shear wave scattering from a nonwelded interface observed by magnetic resonance elastography. *Phys. Med. Biol.* 52, 675–684.
- Papazoglou, S., Hamhaber, U., Braun, J., Sack, I., 2008. Algebraic Helmholtz inversion in planar magnetic resonance elastography. *Phys. Med. Biol.* 53, 3147–3158.
- Pittock, S.J., Lucchinetti, C.F., 2007. The pathology of MS: new insights and potential clinical applications. *Neurologist* 13, 45–56.
- Prange, M.T., Margulies, S.S., 2002. Regional, directional, and age-dependent properties of the brain undergoing large deformation. *J. Biomech. Eng.* 124, 244–252.
- Sack, I., Beierbach, B., Hamhaber, U., Klatt, D., Braun, J., 2008. Non-invasive measurement of brain viscoelasticity using magnetic resonance elastography. *NMR Biomed.* 21, 265–271.
- Sack, I., Beierbach, B., Wuerfel, J., Klatt, D., Hamhaber, U., Papazoglou, S., Martus, P., Braun, J., 2009a. The impact of aging and gender on brain viscoelasticity. *NeuroImage* 46, 652–657.
- Sack, I., Streitberger, K., Hamhaber, U., Klatt, D., Papazoglou, S., Krefling, D., et al., 2009b. Comparison of brain viscoelasticity and brain volumetry in healthy volunteers. *Proc. 17th Scientific Meet., Int. Soc. Magn. Reson. Med. Honolulu* 2507.
- Sinkus, R., Siegmann, K., Xydeas, T., Tanter, M., Claussen, C., Fink, M., 2007. MR elastography of breast lesions: understanding the solid/liquid duality can improve the specificity of contrast-enhanced MR mammography. *Magn. Reson. Med.* 58, 1135–1144.
- Smith, S.M., Zhang, Y., Jenkinson, M., Chen, J., Matthews, P.M., Federico, A., et al., 2002. Accurate, robust, and automated longitudinal and cross-sectional brain change analysis. *NeuroImage* 17, 479–489.
- Van Essen, D.C., 1997. A tension-based theory of morphogenesis and compact wiring in the central nervous system. *Nature* 385, 313–318.
- Wuerfel, J., Bellmann-Strobl, J., Brunecker, P., Aktas, O., McFarland, H., Villringer, A., et al., 2004. Changes in cerebral perfusion precede plaque formation in multiple sclerosis: a longitudinal perfusion MRI study. *Brain* 127, 111–119.
- Wuerfel, J., Haertle, M., Waiczies, H., Tysiak, E., Bechmann, I., Wernecke, K.D., et al., 2008. Perivascular spaces—MRI marker of inflammatory activity in the brain? *Brain* 131, 2332–2340.
- Yin, M., Talwalkar, J.A., Glaser, K.J., Manduca, A., Grimm, R.C., Rossmann, P.J., et al., 2007. Assessment of hepatic fibrosis with magnetic resonance elastography. *Clin. Gastroenterol. Hepatol.* 5, 1207–1213.
- Zipp, F., Aktas, O., 2006. The brain as a target of inflammation: common pathways link inflammatory and neurodegenerative diseases. *Trends Neurosci.* 29, 518–527.